Journal of Pathology
J Pathol June 2024; **263:** 226–241
Published online 4 April 2024 in Wiley Online Library
(wileyonlinelibrary.com) DOI: 10.1002/path.6277

ORIGINAL ARTICLE

Cell division–dependent dissemination following E-cadherin loss underlies initiation of diffuse-type gastric cancer

Jooske L Monster[1], Lars JS Kemp[1,2†], Georg A Busslinger[3†,‡,§], Marjolein J Vliem[1], Lucca LM Derks[1], Annelot AL Staes[1], Tanya M Bisseling[4], Hans Clevers[3¶], Rachel S van der Post[2*] and Martijn Gloerich[1*]

[1] *Center for Molecular Medicine, University Medical Center Utrecht and Utrecht University, Utrecht, The Netherlands*
[2] *Department of Pathology, Radboud University Medical Center, Nijmegen, The Netherlands*
[3] *Hubrecht Institute, Royal Netherlands Academy of Arts and Sciences (KNAW) and University Medical Center Utrecht, Utrecht, The Netherlands*
[4] *Department of Gastroenterology and Hepatology, Radboud University Medical Center, Nijmegen, The Netherlands*

**Correspondence to: RS van der Post, Department of Pathology, Radboud Institute for Molecular Life Sciences, Radboud University Medical Center, Nijmegen 6525GA, The Netherlands. E-mail: chella.vanderpost@radboudumc.nl; M Gloerich, Center for Molecular Medicine, University Medical Center Utrecht, Utrecht 3584CG, The Netherlands. E-mail: m.gloerich@umcutrecht.nl*

†These authors contributed equally to this work.
‡*Present address:* Division of Gastroenterology and Hepatology, Department of Internal Medicine III, Medical University of Vienna, Vienna, Austria
§*Present address:* Research Center for Molecular Medicine (CeMM) of the Austrian Academy of Sciences, Vienna, Austria
¶*Present address:* Pharma, Research and Early Development (pRED) of F. Hoffmann-La Roche Ltd, Basel, Switzerland

Abstract

Loss of the cell–cell adhesion protein E-cadherin underlies the development of diffuse-type gastric cancer (DGC), which is characterized by the gradual accumulation of tumor cells originating from the gastric epithelium in the surrounding stroma. How E-cadherin deficiency drives DGC formation remains elusive. Therefore, we investigated the consequences of E-cadherin loss on gastric epithelial organization utilizing a human gastric organoid model and histological analyses of early-stage DGC lesions. E-cadherin depletion from gastric organoids recapitulates DGC initiation, with progressive loss of a single-layered architecture and detachment of individual cells. We found that E-cadherin deficiency in gastric epithelia does not lead to a general loss of epithelial cohesion but disrupts the spindle orientation machinery. This leads to a loss of planar cell division orientation and, consequently, daughter cells are positioned outside of the gastric epithelial layer. Although basally delaminated cells fail to detach and instead reintegrate into the epithelium, apically mispositioned daughter cells can trigger the gradual loss of the single-layered epithelial architecture. This impaired architecture hampers reintegration of mispositioned daughter cells and enables basally delaminated cells to disseminate into the surrounding matrix. Taken together, our findings describe how E-cadherin deficiency disrupts gastric epithelial architecture through displacement of dividing cells and provide new insights in the onset of DGC.

Keywords: diffuse-type gastric cancer; HDGC; E-cadherin; *CDH1*; human gastric organoids; cell division; spindle orientation; LGN; mitotic extrusion; epithelial reintegration

Received 10 November 2023; Revised 4 January 2024; Accepted 22 February 2024

No conflicts of interest were declared.

Introduction

The architecture of epithelia is strongly intertwined with their function as tissue barriers, which requires their organization into tightly coherent cell layers. Epithelial cohesion and integrity rely on the establishment of intercellular junctions, in which the cell–cell adhesion protein E-cadherin and other members of the classical cadherin family fulfil a central role [1]. Cadherins mechanically couple neighboring cells through homotypic interactions of their extracellular domains, while their cytosolic tails are connected to the actin cytoskeleton through α- and β-catenin [2]. However, the role of the cadherin–catenin complex extends beyond cell adhesion, and through interactions with a plethora of proteins it impinges on cellular processes such as proliferation [3–7], division orientation [8–13], and survival [14–17]. E-cadherin is frequently lost in epithelial cancers, which contributes to the disruption of epithelial organization and metastatic dissemination of cells during late stages of tumor development [18,19]. Pro-oncogenic effects of E-cadherin loss have been

mainly attributed to disrupted cell–cell adhesion, while the contribution of other functions of E-cadherin that impact epithelial organization are less well explored.

In addition to promoting late-stage tumor progression, E-cadherin loss is an early event in specific epithelial cancers and drives the development of diffuse-type gastric cancer (DGC). E-cadherin expression is typically attenuated in sporadic DGC tumors, and mutations in the E-cadherin encoding gene *CDH1* underlie the genetic predisposition to hereditary DGC (HDGC) that arises following inactivation of the remaining wildtype allele [20–24]. Analyses of DGC development in HDGC patients and mouse models revealed that tumor formation is initiated by the dissemination of tumor cells from the single-layered gastric epithelium into the underlying stroma of the mucosa [25–27]. These early-stage intramucosal lesions consist mostly of diffusely spread signet ring cells (SRCs; characterized by their bloated morphology and crescent-shaped nuclei) and can eventually progress into highly infiltrative advanced carcinomas [28]. Cells that have escaped from the epithelium are occasionally found to be still confined by the basement membrane, which is proposed to reflect the initial phase of DGC development [29–32]. In these intraepithelial lesions, the epithelial architecture is lost, as cells are positioned underneath the epithelium (pagetoid spread) or have replaced normal epithelial cells in the gastric gland entirely (*in situ* lesions) [25]. Loss of functional E-cadherin appears to be sufficient for the development of early-stage DGC, as HDGC patients and E-cadherin-deficient mouse models develop many intramucosal DGC lesions throughout their stomach from an early age [28,33–35]. However, it is unknown how E-cadherin loss triggers the detachment of cells from the epithelium and the formation of DGC lesions, and whether this is merely due to disruption of cell–cell adhesion or involves other cellular mechanisms that are affected by the absence of E-cadherin [36].

Here, we investigated how E-cadherin deficiency drives the loss of epithelial organization underlying DGC development, using a human DGC organoid model and histological analyses of HDGC patient tissue. We reveal a central role for cell divisions in the disruption of gastric epithelial architecture upon the loss of E-cadherin, in which daughter cell displacement outside of the epithelial layer induces multilayering and eventually their dissemination into the surrounding matrix. Our results exemplify how dysregulated daughter cell positioning may contribute to tumor initiation by disrupting epithelial architecture and triggering cell dissemination.

Materials and methods

Antibodies and reagents

The following commercial antibodies were used at the indicated concentrations for western blot, immunofluorescence, or immunohistochemistry: mouse anti-E-cadherin (HECD-1; 1:2,500 western blot; ab1416; Abcam, Amsterdam, The Netherlands), mouse anti-α-tubulin (DM1A; 1:5,000 western blot; CP06; Sigma-Aldrich, Amsterdam, The Netherlands), mouse anti-α-catenin (15D9; 1:500 immunofluorescence; ALX-804-101; Enzo Life Sciences, Raamsdonksveer, The Netherlands), mouse anti-P-cadherin (clone 56; 1:100 immunofluorescence and 1:500 western blot; 610227; BD Biosciences, Heidelberg, Germany), rabbit anti-β-catenin (1:500 immunofluorescence; C2206; Sigma-Aldrich), rabbit anti-leucine-glycine-asparagine repeat protein (LGN) (1:250 immunofluorescence and immunohistochemistry; ABT174; Merck, Amsterdam, The Netherlands), mouse anti-E-cadherin (clone 36; 1:500 immunohistochemistry; 610182; BD Biosciences), mouse anti-E-cadherin (NCH-38, Dako Omnis GA059; Agilent, Amstelveen, The Netherlands), and mouse anti-Ki-67 (MIB-1, Dako Omnis GA626; Agilent). The following reagents were used at the indicated concentrations and according to the manufacturer's protocol: RO-3306 (9 μM; Tocris, Abingdon, UK), Y-27632 (10 μM; AbMole BioScience, Brussels, Belgium), and SiR-DNA (1 μM, supplemented with 10 μM verapamil; Spirochrome SC007; Cytoskeleton, Denver, CO, USA).

Human gastric organoid culture and generation of E-cad^{KO} organoids

Gastric organoids, previously derived from isolated whole glands of the human gastric corpus [37], were cultured at 37 °C and 5% CO_2 in basement membrane extract (BME; 3533-010-02; Bio-Techne, Dublin, Ireland) in advanced DMEM/F12 medium (Invitrogen, Bleiswijk, The Netherlands) containing 1% GlutaMax (Invitrogen), 0.01 M HEPES buffer (ThermoFisher Scientific, Bleiswijk, The Netherlands), and 1% penicillin/streptomycin stock solution (Lonza, Oss, The Netherlands), supplemented with 1 × B27 (Invitrogen), 1 × Primocin (Invivogen, Toulouse, France), 1 mM *n*-acetyl cysteine (A9165; Sigma-Aldrich), 2 μM A83-01 (2939/10; Bio-Techne), 200 ng/ml recombinant human FGF10 (100-26; Peprotech, London, UK), 50 ng/ml recombinant human EGF (AF-100-15; Peprotech), 1 nM recombinant Gastrin-I (3533-010-02; Bio-Techne), 0.5 nM Wnt Surrogate-Fc Fusion Protein (U-Protein Express, Utrecht, The Netherlands), R-Spondin1-conditioned medium (5% vol/vol), and Noggin-conditioned medium (10% vol/vol). Organoids were passaged as single cells using trypsin–EDTA (T3924; Sigma-Aldrich) once a week and grown in the presence of Y-27632 for the first 2–3 days; they were kept in culture for a maximum of 15 passages. Organoids were harvested after incubation of 1 mg/ml Dispase II (11510536; ThermoFisher Scientific) for 15 min at 37 °C where indicated.

E-cadherin knock-out organoids were generated by electroporation (as described previously [38]) of the pSpCas9-2A-GFP plasmid (#48138; Addgene, Watertown, MA, USA) containing a sgRNA sequencing targeting exon 3 of the human *CDH1* gene

(sgRNA sequence: 5'-AAGATTGCACCGGTCGACA A-3'). Three days after electroporation, GFP-positive single cells (indicative of Cas9 expression) were purified by fluorescence-activated cell sorting and clonal organoids were expanded. Genomic DNA was isolated from individual clones to genotype for the successful generation of out-of-frame deletion (using the following forward and reverse primers; 5'-TCTTCCCA CAAGTTCGCTCT-3' and 5'-AGTTAAGGCCAGG GATGCTT-3'), which was validated by western blot analysis of whole cell lysates. Stable organoid lines were generated by lentiviral transduction of hEF1α-H2B-mNeonGreen-IRES-Blast (a kind gift from Hugo Snippert, UMCU, The Netherlands [39]) and selection with 7.5 μg/ml blasticidin or hEF1α-E-cadherin-mScarlet-IRES-PURO (NM_001287125.2) and selection with 0.4 μg/ml puromycin.

To monitor the organization of organoids over time (Figure 1B,C and supplementary material, Figures S1B,C and S2D,E), brightfield images of organoids were acquired using an EVOS-M5000 (ThermoFisher Scientific) using a 2× (NA = 0.08), 4× (NA = 0.16), or 10× (NA = 0.4) objective. For the comparison with E-cad^{KO} organoids with ectopically expressed E-cadherin (see supplementary material, Figure S1D,E), brightfield images were made of organoids with junctional E-cadherin-mScarlet signal using a Zeiss Cell Observer (Carl-Zeiss, Breda, The Netherlands) equipped with an Orca Flash 4.0 camera (Hamamatsu, Hamamatsu City, Japan) with a 20× objective (NA = 0.75). For the analysis of organoid morphology, organoids were manually scored for the presence of single cells that were clearly outside of the organoid.

Immunostaining of gastric organoids

For immunostaining, organoids were seeded as single cells in BME drops in glass-bottom dishes (Lab-Tek II; ThermoFisher Scientific). After 7 days of culture (or different time points, where indicated), organoids were fixed in 4% formaldehyde (ThermoFisher Scientific), permeabilized in buffer containing 1% BSA (Sigma-Aldrich), 10% DMSO (VWR Chemicals, Amsterdam, The Netherlands), and 2% Triton X-100 (Sigma-Aldrich) in PBS, and incubated with the indicated primary and Alexa-conjugated secondary antibodies (Life Technologies, ThermoFisher Scientific) together with DAPI (Sigma-Aldrich), and Alexa-conjugated phalloidin (Life technologies) where indicated. For LGN immunostaining in organoids (Figure 3C), cells were stained in suspension following recovery from BME using Dispase (Invitrogen) and subsequent fixation with 4% paraformaldehyde and permeabilization with 0.1% Triton X-100. Immunofluorescence images of whole organoids (Figures 1D,G,I and 3C) were made using a Zeiss LSM880 scanning confocal microscope using a 40× (NA = 1.1) objective (Carl-Zeiss). Shown images are single slices unless stated otherwise.

Immunohistochemistry on patient tissue sections and positional analysis of DGC lesions

FFPE tissue sections (4 μm) from archival patient material (2020–2023) were used from gastrectomy specimens of patients with and without a confirmed pathogenic germline variant in *CDH1*. Immunohistochemistry was performed using the Dako Omnis platform (Agilent Technologies) using an automated staining protocol. H&E-, PAS-diastase (PAS-d)-, and immunohistochemically-stained tissue sections were scanned using a Pannoramic 1000 DX slide scanner (3DHistech, Budapest, Hungary) using a 20× objective or a 40× optical equivalent magnification. Pathological lesions were classified based on histological characteristics as either intraepithelial (Tis; comprising of pagetoid spread and *in situ* lesions within the basement membrane) or early-stage DGC tumors (T1a; SRC carcinomas confined to the mucosa).

For immunofluorescent staining of paraffin-embedded tissue sections (Figures 3D,E and supplementary material, Figure S3C), tissues were dewaxed with xylene and dehydrated by consecutive incubation steps with a decreasing percentage of ethanol. Antigens were retrieved by boiling slides in buffer containing 10 mM TRIS and 1 mM EDTA (pH 9.0). Slides were incubated with the indicated primary and Alexa-conjugated secondary antibodies (Life Technologies) in buffer containing 10% normal goat serum (ThermoFisher Scientific). Tissue sections were mounted in Vectashield with DAPI (Brunschwig, Amsterdam, The Netherlands). Images were made with a Zeiss Cell Observer equipped with Orca Flash 4.0 camera (Hamamatsu) with a 20× objective (NA = 0.75) or a 63× objective (NA = 1.15), or a Zeiss LSM880 scanning confocal microscope using a 63× objective (NA = 1.15) using Zen image acquisition software (Carl-Zeiss).

For the evaluation of the relative location (Figure 2A–C) of the proliferative zone in healthy epithelia (n = 5 non-HDGC patients), intraepithelial lesions, and early-stage DGC lesions (n = 10 HDGC patients), digitized slides were viewed with Sectra Digital Pathology Module, with the use of the built-in image ruler (Sectra, Linköping, Sweden). The relative position along the lumen–pit axis was determined by dividing the absolute position of the proliferative zone of non-pathological glands (marked by Ki-67-positive cells) or the lesions (based on histological analysis) over the total length of the corresponding gastric gland.

RNA expression analysis of classical cadherins

mRNA was isolated from gastric organoids that were grown for 7 days in normal culture conditions and removed from BME with dispase according to the manufacturer's protocol (NucleoSpin RNA; Macherey-Nagel, Dueren, Germany). The mRNA was subsequently converted to cDNA using RT-PCR (iScript™ cDNA Synthesis Kit; BioRad, Lunteren, The Netherlands). The presence of cadherin cDNA was then assessed with PCR (Taq DNA polymerase; New England Biolabs, Ipswich, MA, USA) with

primer pairs for each individual classical cadherin and subsequently run on an agarose gel (see supplementary material, Figure S1F). Primer pairs were validated with mRNA isolated from control cell lines (see supplementary material, Figure S1G; MDA-MB231 for *CDH1, CDH2*, and *CDH3*; HUVEC for *CDH5* and *CDH6*), following the same procedure as described above.

Spindle orientation and cell delamination measurements in gastric organoids

For live-cell imaging of organoids, organoids were seeded, as single cells or as intact organoids following isolation by dispase treatment, in BME drops in glass-bottom dishes (Lab-Tek II; ThermoFisher Scientific). After 7 days of culture, organoids were imaged with a Nikon Spinning Disc confocal microscope using a 40× objective (NA = 1.15; Figures 3A, 4A–C, 5C–E, and supplementary material, Figures S3B and S4A) at 37 °C and 5% CO_2 (Nikon, Amsterdam, The Netherlands). Z-stacks were made in all organoid acquisitions; all analyses were carried out on the three-dimensional shape of the organoid using the Clearvolume plugin [40] of Fiji software [41]. Nuclei were visualized with either SiR-DNA (Figures 3A and supplementary material, Figures S3B and S4A) or H2b-mNeongreen (Figures 4A–C and 5C–F).

Cell division rates of organoids (see supplementary material, Figure S3A) were determined by dividing the number of divisions during the acquisition (17–20 h) by the number of cells present at $t = 0$. Statistical analyses were carried out using Prism 8 software (GraphPad, Boston, MA, USA) using an unpaired *t*-test between the pooled organoid division rates of three independent experiments. The orientation of cell division (Figures 3B and supplementary material, Figure S3B) in Z-stacks of single-layered organoids was scored as the direction of chromosome movement in anaphase in respect to the plane of the epithelial layer based on the position of neighboring nuclei, as planar (∼0–30° angle), tilted (∼31–60° angle), or perpendicular (∼61–90° angle). Statistical analyses were performed using a paired *t*-test in Prism 8 software between the average fraction of planar divisions of three independent experiments. The fate of daughter cells of misoriented (tilted and perpendicular) divisions was monitored for 20 h in total. Disseminated cells where the mode of detachment (five of 34 events) or cell fate (five of 34 cells) was unclear were excluded from analyses. For the visualization of whole organoids (Figure 4A,C), color-coded Z-projections were made using Fiji software [41] and outlines of single cells were segmented using the StarDist plugin [42].

Mitochondrial targeting of cadherins

U2OS cells obtained from the American Type Culture Collection (ATCC, Manassas, VA, USA) were cultured at 37 °C and 5% CO_2 in high-glucose DMEM, supplemented with 10% FBS, and penicillin/streptomycin. Cells were co-transfected with YFP-tagged TPR repeats of human LGN (NM_013296.4, amino acids 8–351 [12]) and mScarlet-tagged mitochondrial surface-binding protein ActA [43] coupled to the cytosolic tail of E-cadherin (NM_009864.2, amino acids 736–888 [12]), N-cadherin (NM_007664.5 amino acids 746–906), P-cadherin (XM_038667222.1, amino acids 678–829), VE-cadherin (NM_001795.5, amino acids 621–784), or K-cadherin (XM_005619465.2, amino acids 566–816). Cells were seeded on collagen-I-coated glass-bottom dishes (Lab-Tek II; ThermoFisher Scientific) after 24 h and live-cell imaging (Figure 3G) was performed after 36–48 h using a Zeiss LSM880 scanning confocal microscope at 37 °C and 5% CO_2 using a 63× objective (NA = 1.15). The fraction of cells with colocalization of LGN to mitochondria (Figure 3H) was scored blindly; a statistical analysis was performed using a paired *t*-test.

MDCK cyst cultures

MDCK GII cells [44] (a kind gift from W. James Nelson, Stanford University, Stanford, CA, USA) were cultured at 37 °C and 5% CO_2 in low-glucose DMEM containing 10% FBS, 1 g/l sodium bicarbonate, and penicillin/streptomycin. Wildtype or E-cadherin^{KO} MDCK cells [45] were grown in three-dimensions as cysts, as described previously [46]. In brief, cells were seeded as single cells in 3.3 mg/ml Matrigel (Corning, Amsterdam, The Netherlands) in glass-bottom dishes (Lab-Tek II; ThermoFisher Scientific) and supplemented with fresh medium every 2–3 days. Cysts were fixed and immunostained (see supplementary material, Figure S3D) after 7 days of culture with the immunostaining protocol for organoids described above.

Results

E-cadherin-deficient gastric organoids display a progressive loss of epithelial architecture

To study the consequences of E-cadherin loss on gastric epithelial architecture, we used human gastric organoids that recapitulate the native organization of the gastric epithelium in a three-dimensional environment [37,47]. We generated E-cadherin-deficient (E-cad^{KO}) gastric organoids using CRISPR/Cas9 genome editing (Figure 1A and supplementary material, Figure S1A). We monitored both wildtype and E-cad^{KO} organoids growing from single cells over time within a matrix of BME, which closely mimics the composition of the basement membrane to which native gastric epithelia adhere (Figure 1B,C) [48]. Wildtype gastric organoids gradually developed from a compact cell cluster into a single layer of polarized epithelial cells surrounding a lumen (typically visible after 3–4 days), visualized by staining of the F-actin cytoskeleton (Figure 1B–D). Surprisingly, a substantial fraction of E-cad^{KO} organoids developed a similar epithelial organization, indicating that gastric organoids lacking E-cadherin remain able to form a

cohesive, polarized epithelial monolayer (Figure 1B–D). However, over time, E-cad^{KO} cultures showed an increased prevalence of organoids that either failed to develop or lost their single-layered organization, resulting in organoids with multiple lumens as well as complete lumen loss (Figure 1B–D). We also observed a progressive accumulation of individual cells outside of E-cad^{KO} organoids that appeared to have detached from the organoid epithelium into the extracellular matrix (Figure 1B–D). A fraction of these cells displayed a bloated morphology with crescent-shaped nuclei (Figure 1D, yellow arrowheads), akin to the characteristically shaped SRCs found in early-stage DGC tumors (Figure 1E; inset). The abundance of detached cells was increased when the basement membrane surrounding mature E-cad^{KO} organoids was disrupted with the matrix protease dispase (see supplementary material, Figure S1B,C), suggesting that the basement membrane

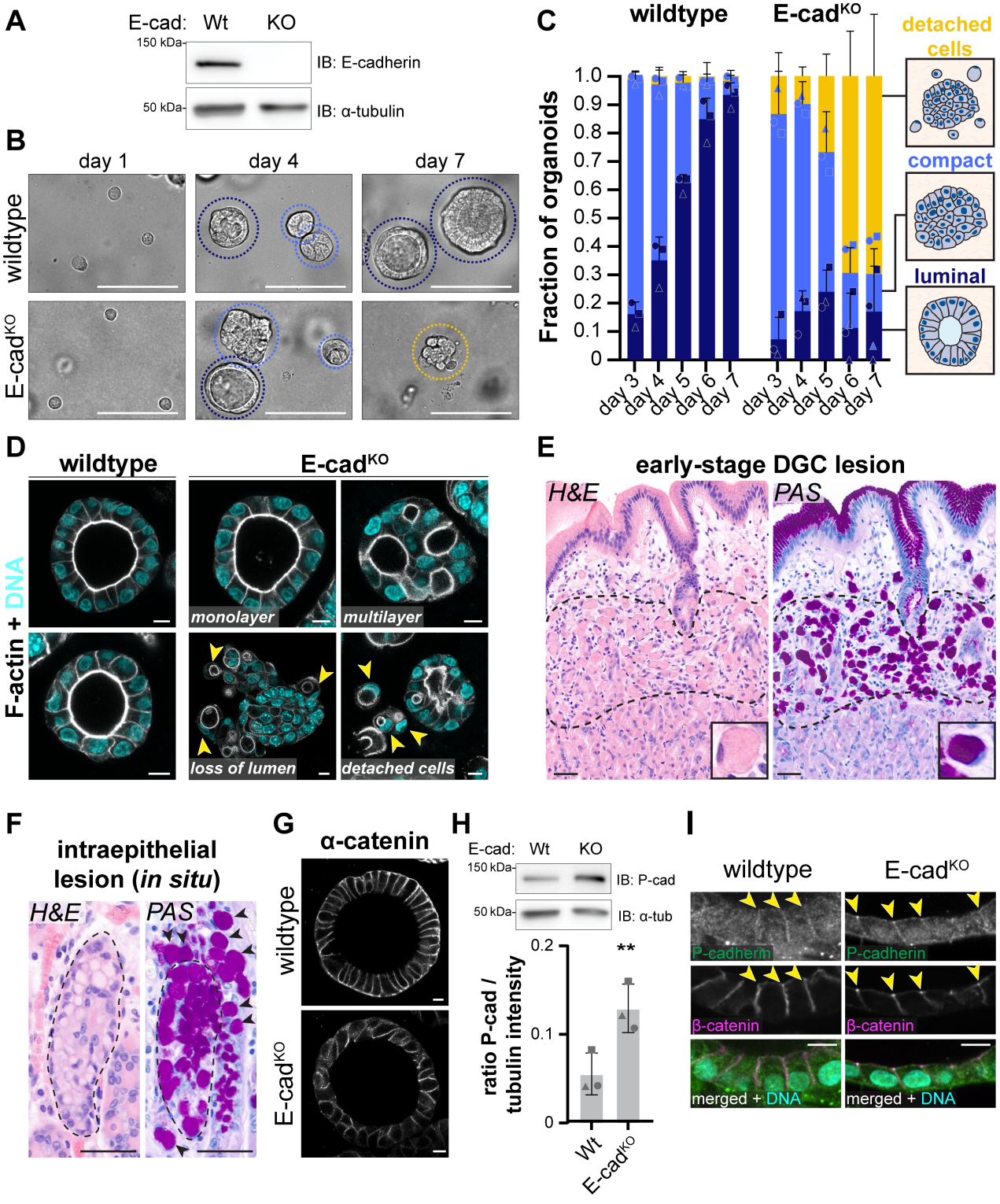

Figure 1 Legend on next page.

may physically hamper cells from leaving the organoid epithelium. Importantly, introduction of ectopic E-cadherin–mScarlet prevented the loss of epithelial architecture and accumulation of detached cells in E-cad^{KO} organoids, validating that the morphological changes observed in E-cad^{KO} organoids are a consequence of the absence of E-cadherin (see supplementary material, Figure S1D,E).

The progressive disruption of epithelial architecture in E-cad^{KO} organoids shows similarities with the histopathological stages in HDGC patients, reflected by intraepithelial lesions that have lost the normal epithelial organization within a gastric gland (Figure 1F) and DGC lesions consisting of tumor cells that have disseminated from the epithelium (Figure 1E). The intraepithelial lesions are presumed to be a precursor stage of DGC tumors in the stroma, underscored by SRCs disseminated in the stroma occasionally being found in close proximity to intraepithelial lesions (Figure 1F). Taken together, our data indicate that E-cadherin deficiency leads to a gradual disruption of gastric epithelial architecture with detachment of individual cells, even though it does not result in a general loss of intercellular adhesion.

We speculated that other adhesion molecules help to retain gastric epithelial cell–cell adhesion in the absence of E-cadherin. In line with this, we observed that core components of the cadherin complex (i.e. α-catenin and β-catenin) remained present at cell–cell contacts in intact E-cad^{KO} organoids (Figure 1G,I), indicating the presence of other cadherin family members in the gastric epithelium in the absence of E-cadherin. Indeed, we detected RNA expression of P-cadherin (but not other classical cadherins; N-, K-, and VE-cadherin) in both wildtype and E-cad^{KO} gastric organoids (see supplementary material, Figure S1F). The presence of P-cadherin was confirmed by western blot analyses and immunostaining, which showed upregulation of P-cadherin protein levels in E-cad^{KO} organoids and the localization of P-cadherin at cell–cell contacts in these organoids (Figure 1H,I). Thus, our data suggest that disruption of the single-layered architecture of the gastric epithelium following E-cadherin loss is not merely due to loss of cell–cell adhesion and probably involves attenuation of additional cellular processes that cannot be compensated for by other cadherin proteins.

Cell detachment from E-cadherin-deficient gastric epithelia is linked to cell proliferation

To understand the potential mechanisms underlying the escape of E-cadherin-deficient cells from the gastric epithelium, we further characterized the earliest stages of tumor development in HDGC patients using histological and immunohistochemical analyses (Figure 2A,B). Analysis of the spatial distribution of intraepithelial lesions (*in situ* lesions and pagetoid spreads) showed a strong bias towards their formation in the isthmus region of gastric glands, typically residing near the proliferative zone that is marked by Ki-67 expression (Figure 2C and supplementary material, Figure S2A). Similarly, early-stage intramucosal DGC lesions closely overlapped with this proliferative region (Figure 2A–C and supplementary material, Figure S2B), as has previously been reported in both DGC patients and mouse models [31,34,35,49]. These data imply that DGC lesions originate from the proliferative region of the gastric epithelium.

One potential explanation for the spatial bias is that the process of cell division itself contributes to disruption of gastric epithelial architecture and cell detachment. To test this hypothesis, we blocked cell division in E-cad^{KO} organoids using the Cdk1 inhibitor RO-3306, which prevents cells from entering mitosis. Organoids were treated with RO-3306 at the approximate moment we typically observed the onset of cell detachment, between days 4 and 5 after plating (Figure 2D,E). This showed that RO-3306-mediated inhibition of cell division fully halts the detachment of cells from E-cad^{KO} organoids (Figure 2D,E). Overall, these data indicate that cell divisions are required for the progressive detachment of cells from gastric organoids and

Figure 1. E-cadherin-deficient human gastric organoids mimic the early-stage development of DGC. (A) Western blot analysis of lysates from parental (Wt) and E-cadherin knock-out (KO) human gastric organoid lines probed (IB, immunoblot) for E-cadherin and α-tubulin. (B) Representative phase-contrast images of wildtype and E-cad^{KO} organoid cultures at 1, 4, and 7 days after seeding as single cells in a BME matrix. Organoids with a visible lumen (dark blue), no lumen (blue), and with detached cells surrounding the organoids (yellow) are indicated by dashed lines. (C) Quantification of wildtype and E-cad^{KO} organoid morphology over time, indicating means ± SD from three independent experiments (individual experiments indicated by shapes). (D) Representative immunostaining of wildtype and E-cad^{KO} organoids after 7 days of culture. To visualize organoid morphology, DNA (DAPI; cyan) and F-actin (phalloidin; grays) were labeled, highlighting the apical brush border surrounding the lumen(s). Yellow arrowheads indicate single cells with a SRC-like morphology, with peripheral crescent-shaped nuclei. (E) H&E and PAS staining on serial sections of an early-stage DGC lesion (outlined with a dashed line) of an HDGC patient, with a high-magnification inset of an individual SRC. Note the intracellular accumulation of mucin (magenta in PAS) that displaces the nucleus to the cell periphery. (F) H&E and PAS staining on serial sections of an *in situ* intraepithelial lesion of an HDGC patient, with SRCs confined within the basement membrane (outlined with a black dashed line) that have largely replaced the normal gastric epithelial cells. In the tissue section stained with PAS, additional SRCs are visible outside the gastric gland (black arrows). (G) Immunostaining of wildtype and E-cad^{KO} organoids for the cadherin complex component α-catenin (grays). Note that although α-catenin is not absent from cell–cell contacts in the absence of E-cadherin, its presence is slightly reduced and more punctuated. (H) Western blot analysis of lysates from parental (Wt) and E-cadherin knock-out (KO) human gastric organoid lines for P-cadherin and α-tubulin. A representative blot and the mean P-cadherin expression levels (normalized to α-tubulin levels) ± SD from three independent experiments (individual experiments indicated by shapes) are shown. Paired *t*-test. $^{**}p < 0.005$. (I) Immunostaining of wildtype and E-cad^{KO} organoids for P-cadherin (green in merge), showing colocalization with β-catenin (magenta in merge) at cell–cell contacts (arrowheads), together with DAPI (cyan). Scale bars, 10 μm (D, G and I) or 100 μm (B, E and F).

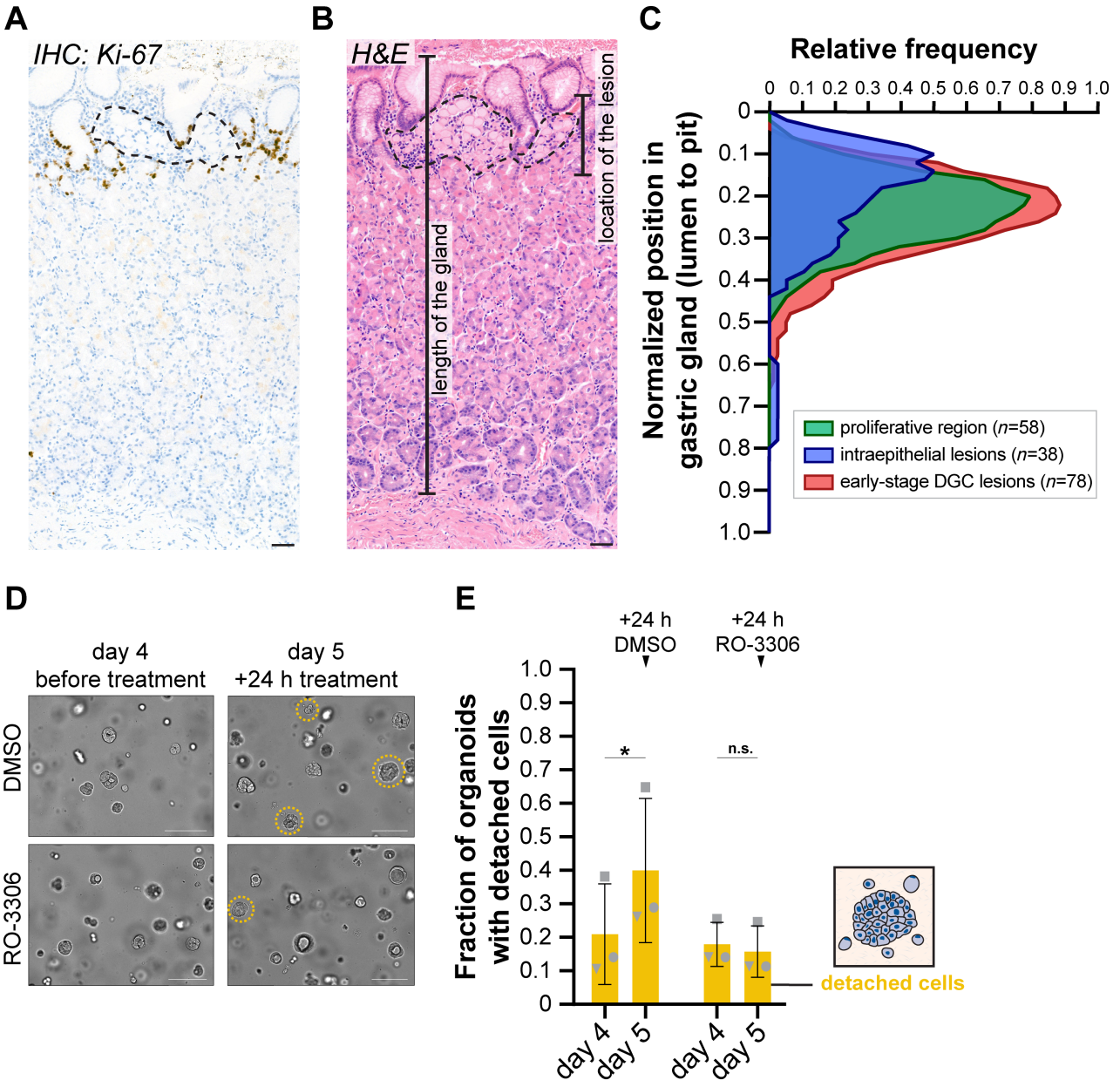

Figure 2. Cell detachment from E-cadherin-deficient gastric epithelia is linked to cell division. (A) Immunohistochemical staining for proliferation marker Ki-67 on a serial section of an early-stage DGC lesion (outlined with a dashed line), showing that the lesion resides near the Ki-67-positive proliferative region of surrounding healthy gastric glands. (B) H&E staining on a serial section of an early-stage DGC lesion (outlined with a dashed line), exemplifying the measurements for the total length of the gastric gland and the location of the lesion used in the quantification (C). (C) Histogram of the relative positions of the proliferative zone (green; marked by Ki-67-positive cells; $n = 58$), intraepithelial lesions (blue; $n = 38$), and early-stage DGC lesions (red; $n = 78$) in the stroma along the lumen–pit axis of gastric epithelial glands of the corpus, relative to the total length of the corresponding gland. The frequency indicates the relative number of lesions or proliferative area present in each region in the gastric gland. (D) Representative examples of phase-contrast images of E-cad^{KO} organoid cultures before or after treatment with RO-3306 that inhibits mitotic entry, or vehicle control DMSO, added following 4 days of culture. Organoids with detached cells surrounding the organoids are indicated with yellow dashed lines. (E) Quantification of the fraction of organoids with detached cells before or 24 h after the addition of DMSO or RO-3306. Mean fractions ± SD of three independent experiments (individual experiments indicated by gray shapes) are shown. Paired *t*-test: n.s. not significant; $^*p < 0.05$. Scale bars, 100 µm.

suggest that this process contributes to the formation of DGC lesions following E-cadherin loss.

Absence of E-cadherin results in randomization of cell division orientation in gastric epithelia

To understand how cell divisions contribute to the loss of epithelial tissue architecture, we followed dividing cells in wildtype and E-cad^{KO} organoids that had not yet lost their single-layered architecture. Using timelapse confocal imaging of organoids with labeled DNA, we could closely assess cell divisions within the three-dimensional epithelium of organoids (see Figure 3A,B and supplementary material, Movies S1–S6). Whereas the number of divisions is not increased in E-cad^{KO} organoids compared with wildtype (see supplementary

material, Figure S3A), we noted a striking difference in the orientation of these divisions. In wildtype organoids, cells consistently oriented their divisions in the plane of the epithelium (Figure 3A,B and supplementary material, Movies S1 and S2), which has been previously shown to be essential for the maintenance of single-layered

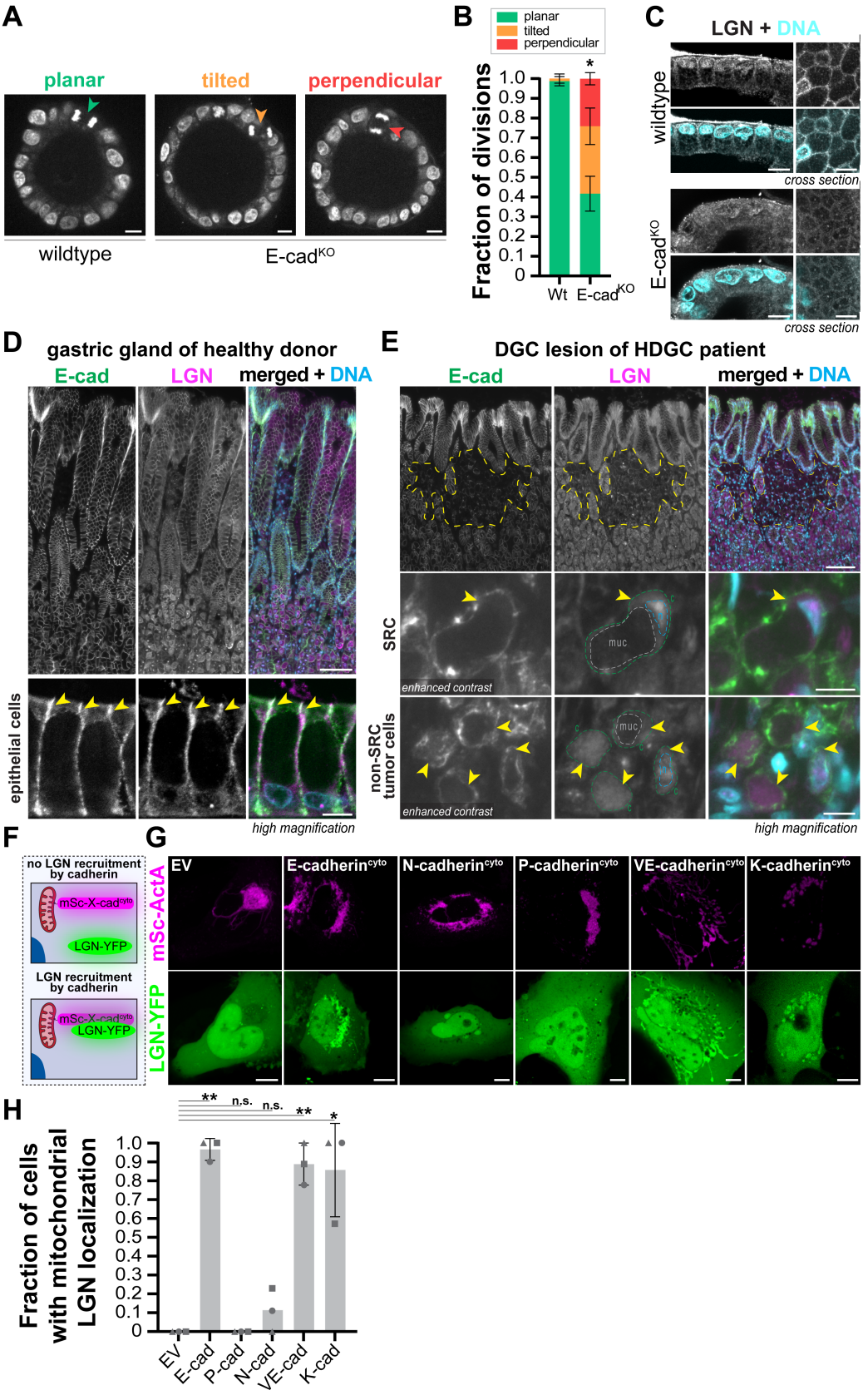

Figure 3 Legend on next page.

epithelial architecture [50]. In E-cad^{KO} organoids, division orientation was not exclusively planar and, instead, divisions were frequently tilted or oriented perpendicular to the epithelial monolayer (Figure 3A,B and supplementary material, Movies S3–S6). Planar cell divisions in E-cad^{KO} organoids were restored upon introduction of ectopic E-cadherin–mScarlet (see supplementary material, Figure S3B). Thus, loss of E-cadherin leads to a disruption of planar divisions and results in a randomized orientation of cell division in gastric organoids.

It has previously been shown that E-cadherin establishes planar cell divisions by recruitment of LGN, a core adaptor protein of the spindle orientation machinery, to ensure planar spindle positioning when cells enter mitosis [12]. Immunostaining for LGN showed that its cortical localization along cell–cell contacts observed in wildtype gastric organoids (Figure 3C) was attenuated in E-cad^{KO} organoids (Figure 3C), in line with their loss of planar cell divisions. To test whether the regulation of LGN is also perturbed during DGC development, we performed immunohistochemical analyses on tissue sections of gastric tissue from healthy individuals and early-stage lesions from HDGC patients. In epithelia of healthy gastric tissue, we observed the localization of LGN at cell–cell adhesions marked by E-cadherin (Figure 3D). In contrast, the cortical distribution of LGN was lost in tumor cells of lesions of HDGC patients with aberrant E-cadherin expression (five of five lesions), in which LGN was instead found in the cytoplasm and nucleus (Figure 3E and supplementary material, Figure S3C). This cytoplasmic accumulation of LGN was particularly apparent in less-differentiated tumor cells, which lack the cytoplasmic mucin vacuoles present in SRCs (Figure 3E and supplementary material, Figure S3C). This shows that in gastric epithelial cells, loss of E-cadherin disrupts the cortical localization of LGN.

As the cortical LGN localization is disrupted upon loss of E-cadherin in gastric organoids (Figure 3D) even though other cadherins are present (Figure 1F–H), this raises the question whether LGN is selectively able to interact with E-cadherin. To test the ability of the different cadherin family members to localize LGN, we artificially targeted their cytosolic tails to mitochondria in U2OS cells (which lack endogenous E-cadherin) and monitored the co-recruitment of ectopically expressed LGN (Figure 3F). This revealed that in addition to E-cadherin, K-cadherin (*CDH6*) and VE-cadherin (*CDH5*) were also capable of targeting LGN to mitochondria (Figure 3G,H). In contrast, the other classical cadherin family member expressed in the gastric epithelium, P-cadherin (*CDH3*; Figure 1H,I and supplementary material, Figure S1F), was not able to recruit LGN (Figure 3G,H), explaining why its presence is insufficient to localize LGN to cell–cell contacts in E-cad^{KO} organoids (Figure 3C). Overall, these data show that loss of E-cadherin in gastric epithelia results in the disruption of planar cell divisions, which is explained by the incapacity of the remaining cadherins to recruit LGN to cell–cell adhesions.

Reintegration of daughter cells from misoriented divisions in single-layered epithelia

Next, we investigated whether misoriented divisions in E-cadherin-deficient gastric organoids position daughter cells outside of the monolayer and thereby contribute to the loss of the single-layered epithelial architecture. For this, we tracked the daughter cells of misoriented cell divisions in E-cad^{KO} organoids, at a stage that they had still retained their single-layered architecture (Figure 4 and supplementary material, Movies S7–S9). We observed that during misoriented divisions, typically one daughter cell remains within the monolayer while

Figure 3. Disruption of planar cell division machinery upon E-cadherin loss. (A) Representative images of the orientation of cell divisions in wildtype and E-cad^{KO} organoids, marked with labeled nuclei (H2b-mNeon). (B) Quantification of the orientation of cell divisions in respect to the plane of the organoid epithelium in wildtype and E-cad^{KO} organoids. The mean fraction of divisions ± SD from three independent experiments with >20 divisions per condition per experiment is shown. Paired *t*-test comparing planar divisions: $^{*}p < 0.05$. (C) Immunostaining (longitudinal view and cross-section) of wildtype and E-cad^{KO} gastric organoids for LGN (grays), together with DAPI (cyan). Of note, some non-specific antibody staining of remnant BME surrounding the organoid is visible for the wildtype organoid (top left). (D) Immunohistochemical analysis of gastric epithelial tissue from a healthy individual for E-cadherin (green) and LGN (magenta), together with DAPI (cyan). High-magnification images (bottom) show that LGN localizes to cell–cell contacts marked by E-cadherin (yellow arrowheads), while being excluded from mucin granules in mucin-secreting cells. (E) Immunohistochemical analysis of an early-stage DGC lesion (marked by a dashed yellow line) of an HDGC patient for E-cadherin (green) and LGN (magenta). High-magnification images below show SRCs (middle panel) and less-differentiated tumor cells lacking the bloated SRC morphology (bottom panel), with attenuated cortical E-cadherin localization. In these cells, LGN has lost its cortical (c; green dashed line) distribution (marked by yellow arrowheads) and is found throughout the cell, frequently enriched in the nucleus (*n*; blue dashed line) that presumably results from its interaction with nuclear NuMA [12]. Note that in many SRCs the cytoplasm is almost completely pushed peripheral by accumulated mucin (muc; gray dashed line; which lacks LGN staining) and, therefore, LGN may appear cortical. In five of five lesions from three HDGC patients the loss of cortical LGN was observed (see supplementary material, Figure S3C). (F) Schematic illustration of a mitochondrial targeting assay to assess cadherin–LGN interactions, by localization of the cytosolic tails of cadherins labeled with mScarlet (mSc) and determining the recruitment of the YFP-tagged TPR domain of LGN that binds E-cadherin (abbreviated to LGN-YFP) [12]. (G) Representative images of a mitochondrial targeting assay to determine cadherin–LGN association in U2OS cells. The top panels show mitochondrial localization (magenta) of the respective cadherin cytosolic tails or empty vector (EV); the bottom panels show the localization of LGN (green). (H) Quantification of the relative recruitment of YFP-LGN to mitochondria by the cytosolic tail of different cadherin family members. The mean fraction of cells with mitochondrial localization of LGN ± SD of three independent experiments (individual experiments indicated by gray shapes) is shown. Paired *t*-tests compared with EV: n.s. not significant; $^{*}p < 0.05$; $^{**}p < 0.005$. Scale bars, 10 μm (A, C and G and bottom panels of D and E) or 100 μm (top panel of D and E).

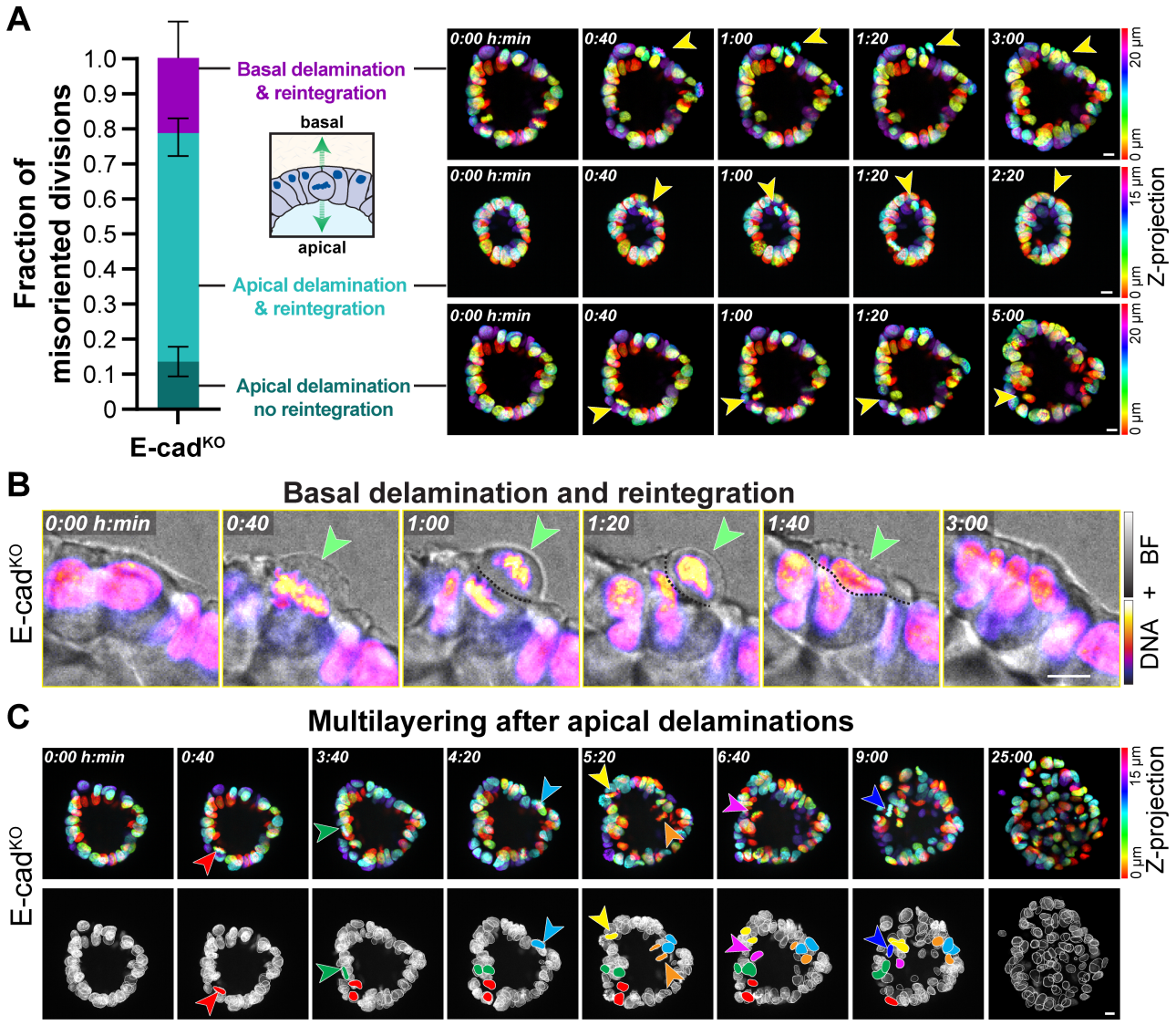

Figure 4. Misoriented divisions can reintegrate in the gastric epithelium or result in multilayering. (A) Analysis of the position of daughter cells from misoriented divisions in gastric E-cad^{KO} organoids. The quantification shows the average distribution ± SD from three independent experiments (38 misoriented divisions). Examples for each category are shown in a color-coded Z-projection (four or five slices with a 5 µm interval) of the organoid with marked nuclei (H2b-mNeon) at indicated timepoints; dividing cells are highlighted with yellow arrowheads. (B) High-magnification examples of a basally delaminated cell (from A) that reintegrates in the E-cad^{KO} organoid epithelial layer. The time-series of brightfield images with marked nuclei (H2b-mNeon, Fire LUT) shows that the daughter cell of misoriented divisions (green arrowheads) can retain an adhesive surface contact (indicated with a dashed line), which expands upon their reintegration. (C) Example of a time-series of a color-coded Z-projection (four slices with a 5 µm interval) of an E-cad^{KO} organoid that progressively loses the epithelial monolayer due to apically mispositioned daughter cells that fail to reintegrate. Individual misoriented divisions are marked by arrowheads and their respective daughter cells are marked over time in the bottom panel. Scale bars, 10 µm.

the other daughter cell is positioned outside the epithelial layer, with an increased propensity to localize apically over basally (77% versus 23%) (Figure 4A). Strikingly, instead of disseminating into the surrounding matrix, the majority of cells that delaminate from the epithelium reintegrated in the monolayer within several hours (Figure 4A,B and supplementary material, Movies S7 and S8). Misplaced daughter cells of non-planar divisions typically retained a region of contact with cells of the monolayer; after the completion of mitosis, this contact expanded and the delaminated cell moved back into the epithelium (Figure 4B and supplementary material, Movies S7 and S8). This occurred for all cells that delaminated on the basal side of the epithelium (Figure 4A), even in the absence of a basement membrane following dispase treatment (data not shown). Importantly, a fraction (16%) of apically delaminated cells remained outside the epithelial monolayer (Figure 4A and supplementary material, Movie S9). These apically delaminated cells that did not reintegrate caused the multilayering of the organoid epithelium; misoriented divisions were typically the initiating event towards complete loss of epithelial architecture and lumen loss (Figure 4C and supplementary material, Movie S9). Thus, although non-planar divisions can position daughter cells out of the epithelium, this process by itself does

not result in complete detachment of cells from the gastric organoid epithelium into the surrounding matrix because delaminated cells reintegrate into the monolayer. However, misoriented divisions can lead to the multilayering and eventual complete loss of epithelial architecture.

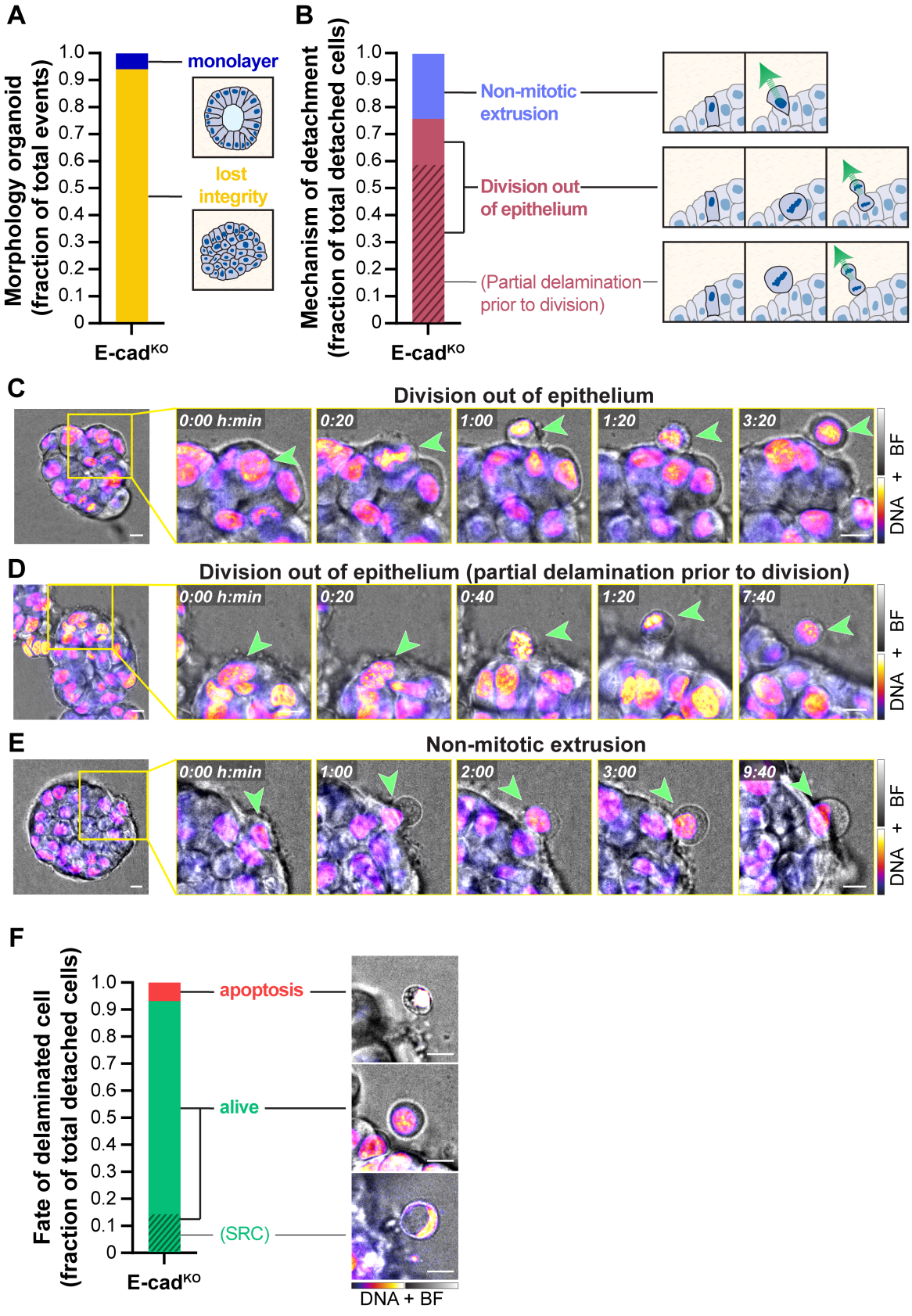

Figure 5 Legend on next page.

Aberrant positioning of daughter cells triggers cell dissemination from organoids that have lost their single-layered architecture

Our data indicate that loss of planar divisions is insufficient to drive the basal detachment of cells from gastric E-cad^{KO} organoids that still have a single-layered architecture. Therefore, to understand the origin of disseminated cells (Figure 1D), we followed the growth of E-cad^{KO} organoids starting from a single-layered epithelium until cell detachments were observed (Figure 5 and supplementary material, Movies S10–S12). This revealed that complete cell detachments into the surrounding matrix almost exclusively occurred after the single-layered architecture was disrupted (i.e. multilayered or total loss of lumen; Figure 5A and supplementary material, Movies S10–S12). When further characterizing these cell-dissemination events in E-cad^{KO} organoids, we noticed that the majority (22 of 29) of detached cells directly originated from dividing cells (Figure 5B). This was due to cell divisions in the outer layer of the organoid resulting in the positioning of one of the daughter cells outside of the organoid, at sufficient distance to completely lose contact and prevent reintegration (Figure 5B–D and supplementary material, Movies S10 and S11). These cells were frequently already positioned partially outside the epithelium prior to cell division, predominantly due to the basal movement of cells to the periphery of the E-cad^{KO} organoid following mitotic entry (Figure 5B,D and supplementary material, Movie S11). This partial delamination prior to division presumably decreases the likelihood of their integration by increasing the distance between daughter cells and the organoid epithelium, and thereby limiting the remaining surface contact between them. Although we also observed a small fraction of extrusions originating from non-mitotic cells (Figure 5B,E and supplementary material, Movie S12), the majority of events where cells completely disseminated from E-cad^{KO} organoids is dependent on the aberrant positioning of daughter cells following cell division (Figure 5B), and this requires the preceding loss of the epithelial monolayer.

Following basal detachment into the extracellular matrix, the majority of E-cadherin-deficient cells remained alive, as only a small fraction of cells underwent apoptosis (as determined by nuclear fragmentation; Figure 5F). We did not observe any divisions in disseminated cells, and a fraction of these cells developed into SRC-like cells over time (Figure 5F and supplementary material, Figure S4A and Movie S13). This demonstrates that SRC-like cells observed in the extracellular matrix (Figure 1D) can indeed originate from cells detaching from gastric organoids. Overall, these data show that, following the loss of the monolayered architecture by misoriented divisions, mitotic events also contribute to the dissemination of cells from the gastric epithelium into the surrounding matrix.

Discussion

Here we describe how E-cadherin loss leads to a disruption of gastric epithelial architecture and induction of cell dissemination, which relies on cells to proceed through mitosis. Due to randomization of the orientation of cell division, daughter cells are positioned both basally and apically outside of the epithelial layer. Although basally delaminated cells reintegrate into the single-layered epithelium preventing their dissemination, apically delaminated daughter cells induce a gradual loss of the single-layered epithelial architecture. At this stage, mispositioned daughter cells fail to reintegrate, resulting in the dissemination of basally delaminated cells into the surrounding matrix. Together, our findings underscore that the role of E-cadherin in epithelial organization extends beyond establishing epithelial cohesion and show how E-cadherin deficiency can disrupt epithelial architecture through the displacement of dividing cells. As such, our study exemplifies how dysregulated daughter cell positioning can contribute to tumor initiation, which may represent a mechanism more broadly employed during dissemination of tumor cells from epithelial tissues across different cancer subtypes.

Figure 5. Disseminated cells originate from mispositioned mitotic daughter cells. (A) Quantification of the morphology of E-cad^{KO} organoids at the time of basal cell detachment. The fractions were calculated from the total number of detached cells ($n = 34$) pooled from four independent experiments. (B) Quantification of the mechanism of detachment of cells from E-cad^{KO} organoids, from the total number of detached cells ($n = 29$) pooled from four independent experiments. (C) High-magnification example of a cell dividing out of the E-cad^{KO} organoid. The time-series of brightfield images with marked nuclei (H2b-mNeon, Fire LUT) shows a dividing cell within the organoid resulting in one daughter cell positioned and remaining in the surrounding matrix (green arrowheads). (D) High-magnification example of a cell dividing out of the E-cad^{KO} organoid epithelial layer that was partially delaminated prior to division. The time-series of brightfield images with marked nuclei (H2b-mNeon, Fire LUT) shows a dividing cell within the organoid moving basally after mitotic rounding (between nuclear envelope breakdown; timepoint 0:20 and metaphase; timepoint 0:40). Following division, one daughter cell remains outside the epithelium (green arrowheads), whereas the other daughter cell reintegrates in the monolayer (not shown). (E) High-magnification example of non-mitotic cell dissemination from an E-cad^{KO} organoid epithelial layer. The time-series of brightfield images with marked nuclei (H2b-mNeon, Fire LUT) shows the detachment of the cell from the epithelium in the absence of entry into mitosis (green arrowheads). (F) Quantification and examples of the fates of cells detached from E-cad^{KO} organoids into the surrounding matrix. Representative brightfield images with marked nuclei (H2b-mNeon, Fire LUT) show apoptotic cells (fragmented nuclei; top) and alive cells (no fragmented nuclei, middle and bottom). A subset of alive cells develops into SRC-like cells (crescent-shaped, peripheral nuclei; bottom). Cells were followed for up to 30 h following detachments; fractions were calculated from the total number of detached cells ($n = 29$) pooled from four independent experiments. Scale bars, 10 μm.

The human gastric organoid model in which E-cadherin is depleted provides a powerful tool to study the cellular events underlying the formation of DGC lesions in real-time, as it reflects the genetic and histopathological features of early-stage DGC [37,47,51]. E-cadherin loss is the most established driver event of DGC initiation, and both E-cadherin-deficient organoids and early-stage lesions in HDGC patients display accumulation of cells that disseminated from the basal side of the gastric epithelium and develop into SRCs. In both, dissemination appears to be preceded by a progressive loss of epithelial monolayer architecture, which in patients is reflected by intraepithelial lesions that are found in close proximity to SRC lesions. Our findings thereby support the model of (H)DGC pathogenesis from Carneiro *et al* [30], with DGC development starting with intraepithelial lesions that are the origin of disseminating cells that form the SRC lesions in the stroma. Our detailed analysis of E-cadherin-deficient organoids provides evidence that this process results from mispositioning of daughter cells, which is corroborated by histological analysis of HDGC lesions in patients that are associated with cell divisions and disruption of the cell division orientation machinery. Nonetheless, future studies using *in vivo* models of DGC are needed to address to what extent the displacement of dividing cells underlies the formation of initial intraepithelial and subsequent mucosal lesions. These studies will also answer how specific characteristics of native gastric tissue, including the physical properties of the basement membrane and stroma surrounding epithelia, influence epithelial disorganization and tumor cell dissemination during DGC development. Although our study focused on the formation of early-stage DGC lesions, it remains unanswered whether advanced DGC originates from the malignant transition of these early lesions or constitutes an independent event [36]. Importantly, in both scenarios the development of advanced tumors relies on the prior dissemination of cells from the gastric epithelium.

Our data indicate that E-cadherin loss is insufficient to drive a complete loss of cohesion in gastric epithelia, presumably due to the presence of other adhesion molecules. Instead, the progressive disruption of architecture and cell detachments from E-cadherin-deficient epithelia arise from mispositioning of daughters of cell divisions. The physical displacement of newly formed daughter cells following division may challenge the cell–cell contacts between E-cadherin-deficient cells and thereby lead to detachment (Figure 5). The positioning of daughter cells is determined by the orientation of cell division, which is tightly controlled throughout epithelial development and homeostasis [52,53]. As such, division orientation ensures that simple epithelia maintain their monolayered architecture and conversely induces multilayering of stratified epithelia [50,54]. Our data indicate that loss of the regulation of cell division orientation represents an oncogenic event, which is supported by previous studies that linked misoriented cell divisions to tumor formation in *Drosophila* wing disc epithelia [55,56] and prostate tumorigenesis in mouse models [13]. It has previously been demonstrated that cell division orientation is regulated by E-cadherin independent of its function in cell–cell adhesion [12]. Importantly, this does not exclude that the absence of E-cadherin could weaken cell–cell adhesion, as also suggested by junctional α-catenin localization being slightly reduced and more punctuated in E-cad^{KO} compared with wildtype organoids (Figure 1G). This potentially reduced adhesiveness could contribute to the epithelial disorganization and cell dissemination following cell divisions, and different functions of E-cadherin may act in concert to maintain gastric epithelial architecture.

We found that the gastric epithelium has intrinsic self-organizing properties to protect against the consequences of misoriented divisions by reintegration of delaminated cells into the monolayer, as previously described in *Drosophila* epithelia [57,58]. This protective reintegration mechanism in *Drosophila* epithelia was shown to be mediated by the interaction of displaced daughter cells with the epithelial layer through lateral adhesion molecules, and a similar mechanism may guide cellular reintegration in the mammalian gastric epithelium. As we observe dissemination of E-cadherin-deficient cells only after the monolayer architecture is lost, the mechanisms of reintegration may be less efficient in disorganized epithelia. The efficiency of reintegration is presumably influenced by the remaining adhesive surface of mispositioned daughter cells and the epithelium following division. The extent of the remaining adhesive surface probably depends on the distance at which dividing cells are displaced, which may be increased in bulging organoids upon loss of the epithelial architecture. Moreover, mitotic daughter cell displacement can be promoted by the partial delamination of cells upon mitotic entry that we occasionally observed in E-cadherin-deficient organoids. This partial delamination could be a result of weakened intercellular adhesion following E-cadherin loss, as extrusion of mitotic cells has previously been linked to attenuated cell–cell adhesion [59].

This study exemplifies how cadherin family members can have specific binding partners, as we show LGN is exclusively recruited to E-, VE-, and K-cadherin, but not N- and P-cadherin. This suggests that E-cadherin loss will distinctly affect division orientation across different epithelia, dependent on the repertoire of cadherin proteins they express. Indeed, in contrast to gastric epithelia, E-cadherin loss is insufficient to disrupt junctional LGN localization and planar cell divisions in MDCK cells that also express K-cadherin (see supplementary material, Figure S3D; [10,60,61]). Understanding which functions of E-cadherin are shared with other cadherin family members, as well as the divergent expression of cadherins across epithelial tissues of different organs, will help to explain why patients with a germline mutation in *CDH1* are predisposed to develop tumors in specific organs, such as in the stomach.

Acknowledgements

We thank Willem-Jan Pannekoek and Madelon Maurice (UMC Utrecht, The Netherlands) for critical reading of the manuscript and members of our laboratory for the helpful discussions throughout the project. This work was supported by the Dutch Cancer Foundation (KWF-12345) and the Netherlands Organization for Scientific Research (NWO; 016.Vidi.189.166, NWO gravitational program CancerGenomiCs.nl 024.001.028, and the Science-XL research program The Active Matter Physics of Collective Metastasis 2019.022).

Author contributions statement

JLM, RSP and MG conceived the study. GAB and HC provided human gastric organoids and generated E-cadherin knock-out organoids. JLM, LJSK, MJV, LLMD, AALS, GAB and RSP performed experiments and analyzed data. TMB provided the patient material. JLM and MG wrote the manuscript with input and final approval from all the authors. RSP and MG supervised the study.

Data availability statement

The data that support the findings of this study are available on reasonable request by contacting the corresponding authors.

References

1. Baum B, Georgiou M. Dynamics of adherens junctions in epithelial establishment, maintenance, and remodeling. *J Cell Biol* 2011; **192:** 907–917.
2. Mège RM, Ishiyama N. Integration of cadherin adhesion and cytoskeleton at adherens junctions. *Cold Spring Harb Perspect Biol* 2017; **9:** 1–18.
3. Benham-Pyle BW, Pruitt BL, Nelson WJ. Cell adhesion. Mechanical strain induces E-cadherin-dependent Yap1 and β-catenin activation to drive cell cycle entry. *Science* 2015; **348:** 1024–1027.
4. Donker L, Houtekamer R, Vliem M, *et al*. A mechanical G2 checkpoint controls epithelial cell division through E-cadherin-mediated regulation of Wee1-Cdk1. *Cell Rep* 2022; **41:** 111475.
5. Qian X, Karpova T, Sheppard AM, *et al*. E-cadherin-mediated adhesion inhibits ligand-dependent activation of diverse receptor tyrosine kinases. *EMBO J* 2004; **23:** 1739–1784.
6. Perrais M, Chen X, Perez-Moreno M, *et al*. E-cadherin homophilic ligation inhibits cell growth and epidermal growth factor receptor signaling independently of other cell interactions. *Mol Biol Cell* 2007; **18:** 2013–2025.
7. Kim N-G, Koh E, Chen X, *et al*. E-cadherin mediates contact inhibition of proliferation through hippo signaling-pathway components. *Proc Natl Acad Sci U S A* 2011; **108:** 11930–11935.
8. Lu B, Roegiers F, Jan LY, *et al*. Adherens junctions inhibit asymmetric division in the drosophila epithelium. *Nature* 2001; **409:** 522–525.
9. Le Borgne R, Bellaïche Y, Schweisguth F. Drosophila E-cadherin regulates the orientation of asymmetric cell division in the sensory organ lineage. *Curr Biol* 2002; **12:** 95–104.
10. den Elzen N, Buttery CV, Maddugoda MP, *et al*. Cadherin adhesion receptors orient the mitotic spindle during symmetric cell division in mammalian epithelia. *Mol Biol Cell* 2009; **20:** 3740–3750.
11. Inaba M, Yuan H, Salzmann V, *et al*. E-cadherin is required for centrosome and spindle orientation in drosophila male germline stem cells. *PLoS One* 2010; **5:** e12473.
12. Gloerich M, Bianchini JM, Siemers KA, *et al*. Cell division orientation is coupled to cell-cell adhesion by the E-cadherin/LGN complex. *Nat Commun* 2017; **8:** 13996.
13. Wang X, Dong B, Zhang K, *et al*. E-cadherin bridges cell polarity and spindle orientation to ensure prostate epithelial integrity and prevent carcinogenesis in vivo. *PLoS Genet* 2018; **14:** e1007609.
14. Derksen PWB, Liu X, Saridin F, *et al*. Somatic inactivation of E-cadherin and p53 in mice leads to metastatic lobular mammary carcinoma through induction of anoikis resistance and angiogenesis. *Cancer Cell* 2006; **10:** 437–449.
15. Fouquet S, Lugo-Martínez VH, Faussat AM, *et al*. Early loss of E-cadherin from cell-cell contacts is involved in the onset of anoikis in enterocytes. *J Biol Chem* 2004; **279:** 43061–43069.
16. Ferreira AC, Suriano G, Mendes N, *et al*. E-cadherin impairment increases cell survival through notch-dependent upregulation of Bcl-2. *Hum Mol Genet* 2012; **21:** 334–343.
17. Lowy AM, Knight J, Groden J. Restoration of E-cadherin/beta-catenin expression in pancreatic cancer cells inhibits growth by induction of apoptosis. *Surgery* 2002; **132:** 141–148.
18. Perl A-K, Wilgenbus P, Dahl U, *et al*. A causal role for E-cadherin in the transition from adenoma to carcinoma. *Nature* 1998; **392:** 190–193.
19. Birchmeier W, Behrens J. Cadherin expression in carcinomas: role in the formation of cell junctions and the prevention of invasiveness. *Biochim Biophys Acta* 1994; **1198:** 11–26.
20. Becker KF, Atkinson MJ, Reich U, *et al*. E-cadherin gene mutations provide clues to diffuse type gastric carcinomas. *Cancer Res* 1994; **54:** 3845–3852.
21. Machado JC, Oliveira C, Carvalho R, *et al*. E-cadherin gene (CDH1) promoter methylation as the second hit in sporadic diffuse gastric carcinoma. *Oncogene* 2001; **20:** 1525–1528.
22. Guilford P, Hopkins J, Harraway J, *et al*. E-cadherin germline mutations in familial gastric cancer. *Nature* 1998; **392:** 402–405.
23. Tamura G, Yin J, Wang S, *et al*. E-cadherin gene promoter hypermethylation in primary human gastric carcinomas. *J Natl Cancer Inst* 2000; **92:** 569–573.
24. Suriano G, Yew S, Ferreira P, *et al*. Characterization of a recurrent germ line mutation of the E-cadherin gene: implications for genetic testing and clinical management. *Clin Cancer Res* 2005; **11:** 5401–5409.
25. van der Post RS, Gullo I, Oliveira C, *et al*. Histopathological, molecular, and genetic profile of hereditary diffuse gastric cancer: current knowledge and challenges for the future. *Adv Exp Med Biol* 2016; **908:** 371–391.
26. Humar B, Guilford P. Hereditary diffuse gastric cancer: a manifestation of lost cell polarity. *Cancer Sci* 2009; **100:** 1151–1157.
27. Blair VR, McLeod M, Carneiro F, *et al*. Hereditary diffuse gastric cancer: updated clinical practice guidelines. *Lancet Oncol* 2020; **21:** e386–e397.
28. Huntsman DG, Carneiro F, Lewis FR, *et al*. Early gastric cancer in young, asymptomatic carriers of germ-line E-cadherin mutations. *N Engl J Med* 2001; **344:** 1904–1909.
29. Tsugeno Y, Nakano K, Nakajima T, *et al*. Histopathologic analysis of signet-ring cell carcinoma in situ in patients with hereditary diffuse gastric cancer. *Am J Surg Pathol* 2020; **44:** 1204–1212.
30. Carneiro F, Huntsman DG, Smyrk TC, *et al*. Model of the early development of diffuse gastric cancer in E-cadherin mutation carriers

and its implications for patient screening. *J Pathol* 2004; **203:** 681–687.
31. Humar B, Blair V, Charlton A, *et al*. E-cadherin deficiency initiates gastric signet-ring cell carcinoma in mice and man. *Cancer Res* 2009; **69:** 2050–2056.
32. Barber M, Save V, Carneiro F, *et al*. Histopathological and molecular analysis of gastrectomy specimens from hereditary diffuse gastric cancer patients has implications for endoscopic surveillance of individuals at risk. *J Pathol* 2008; **216:** 286–294.
33. Blair V, Martin I, Shaw D, *et al*. Hereditary diffuse gastric cancer: diagnosis and management. *Clin Gastroenterol Hepatol* 2006; **4:** 262–275.
34. Mimata A, Fukamachi H, Eishi Y, *et al*. Loss of E-cadherin in mouse gastric epithelial cells induces signet ring-like cells, a possible precursor lesion of diffuse gastric cancer. *Cancer Sci* 2011; **102:** 942–950.
35. Hayakawa Y, Ariyama H, Stancikova J, *et al*. Mist1 expressing gastric stem cells maintain the normal and neoplastic gastric epithelium and are supported by a perivascular stem cell niche. *Cancer Cell* 2015; **28:** 800–814.
36. Monster JL, Kemp LJS, Gloerich M, *et al*. Diffuse gastric cancer: emerging mechanisms of tumor initiation and progression. *Biochim Biophys Acta Rev Cancer* 2022; **1877:** 188719.
37. Bartfeld S, Bayram T, van de Wetering M, *et al*. In vitro expansion of human gastric epithelial stem cells and their responses to bacterial infection. *Gastroenterology* 2015; **148:** 126–136.e6.
38. Fujii M, Matano M, Nanki K, *et al*. Efficient genetic engineering of human intestinal organoids using electroporation. *Nat Protoc* 2015; **10:** 1474–1485.
39. Verissimo CS, Overmeer RM, Ponsioen B, *et al*. Targeting mutant RAS in patient-derived colorectal cancer organoids by combinatorial drug screening. *Elife* 2016; **5:** e18489.
40. Royer LA, Weigert M, Günther U, *et al*. ClearVolume: open-source live 3D visualization for light-sheet microscopy. *Nat Methods* 2015; **12:** 480–481.
41. Schindelin J, Arganda-Carreras I, Frise E, *et al*. Fiji: an open-source platform for biological-image analysis. *Nat Methods* 2012; **9:** 676–682.
42. Schmidt U, Weigert M, Broaddus C, *et al*. In *Cell Detection with Star-Convex Polygons BT - Medical Image Computing and Computer Assisted Intervention – MICCAI 2018*, Frangi AF, Schnabel JA, Davatzikos C, *et al*. (eds). Springer International Publishing: Cham, 2018; 265–273.
43. Pistor S, Chakraborty T, Niebuhr K, *et al*. The ActA protein of listeria monocytogenes acts as a nucleator inducing reorganization of the actin cytoskeleton. *EMBO J* 1994; **13:** 758–763.
44. Mays RW, Siemers KA, Fritz BA, *et al*. Hierarchy of mechanisms involved in generating Na/K-ATPase polarity in MDCK epithelial cells. *J Cell Biol* 1995; **130:** 1105–1115.
45. Koirala R, Priest AV, Yen C-F, *et al*. Inside-out regulation of E-cadherin conformation and adhesion. *Proc Natl Acad Sci U S A* 2021; **118:** 1–12.
46. Debnath J, Muthuswamy SK, Brugge JS. Morphogenesis and oncogenesis of MCF-10A mammary epithelial acini grown in three-dimensional basement membrane cultures. *Methods* 2003; **30:** 256–268.
47. Nanki K, Toshimitsu K, Takano A, *et al*. Divergent routes toward Wnt and R-spondin niche independency during human gastric carcinogenesis. *Cell* 2018; **174:** 856–869.e17.
48. Arnaoutova I, George J, Kleinman HK, *et al*. Basement membrane matrix (BME) has multiple uses with stem cells. *Stem Cell Rev Rep* 2012; **8:** 163–169.
49. Humar B, Fukuzawa R, Blair V, *et al*. Destabilized adhesion in the gastric proliferative zone and c-Src kinase activation mark the development of early diffuse gastric cancer. *Cancer Res* 2007; **67:** 2480–2489.
50. Ragkousi K, Gibson MC. Cell division and the maintenance of epithelial order. *J Cell Biol* 2014; **207:** 181–188.
51. Togasaki K, Sugimoto S, Ohta Y, *et al*. Wnt signaling shapes the histologic variation in diffuse gastric cancer. *Gastroenterology* 2021; **160:** 823–830.
52. Macara IG, Guyer R, Richardson G, *et al*. Epithelial homeostasis. *Curr Biol* 2014; **24:** R815–R825.
53. Lechler T, Mapelli M. Spindle positioning and its impact on vertebrate tissue architecture and cell fate. *Nat Rev Mol Cell Biol* 2021; **22:** 691–708.
54. Lechler T, Fuchs E. Asymmetric cell divisions promote stratification and differentiation of mammalian skin. *Nature* 2005; **437:** 275–280.
55. Guilgur LG, Prudêncio P, Ferreira T, *et al*. Drosophila aPKC is required for mitotic spindle orientation during symmetric division of epithelial cells. *Development* 2012; **139:** 503–513.
56. Nakajima Y-I, Meyer EJ, Kroesen A, *et al*. Epithelial junctions maintain tissue architecture by directing planar spindle orientation. *Nature* 2013; **500:** 359–362.
57. Bergstralh DT, Lovegrove HE, St JD. Lateral adhesion drives reintegration of misplaced cells into epithelial monolayers. *Nat Cell Biol* 2015; **17:** 1497–1503.
58. Cammarota C, Finegan TM, Wilson TJ, *et al*. An axon-pathfinding mechanism preserves epithelial tissue integrity. *Curr Biol* 2020; **30:** 5049–5057.e3.
59. Ganier O, Schnerch D, Oertle P, *et al*. Structural centrosome aberrations promote non-cell-autonomous invasiveness. *EMBO J* 2018; **37:** e98576.
60. Capaldo CT, Macara IG. Depletion of E-cadherin disrupts establishment but not maintenance of cell junctions in Madin-Darby canine kidney epithelial cells. *Mol Biol Cell* 2007; **18:** 189–200.
61. Stewart DB, Barth AIM, Nelson WJJ. Differential regulation of endogenous cadherin expression in Madin-Darby canine kidney cells by cell-cell adhesion and activation of β-catenin signaling. *J Biol Chem* 2000; **275:** 20707–20716.

SUPPLEMENTARY MATERIAL ONLINE

Figure S1. Characterization of E-cad^{KO} organoids

Figure S2. Localization of intraepithelial and early-stage intramucosal DGC lesions near the proliferative region

Figure S3. Consequences of E-cadherin loss in gastric and renal epithelia

Figure S4. Development of disseminated cells into SRC-like cells

Movie S1. Example of a planar cell division (marked by a yellow arrowhead) in a wildtype organoid, visualized by labeled nuclei (H2b-mNeon)

Movie S2. Three-dimensional visualization of a planar cell division (marked by a yellow arrowhead) in a wildtype organoid, visualized by labeled nuclei (H2b-mNeon)

Movie S3. Example of a tilted cell division (marked by a yellow arrowhead) in an E-cad^{KO} organoid, visualized by labeled nuclei (H2b-mNeon)

Movie S4. Three-dimensional visualization of a tilted cell division (marked by a yellow arrowhead) in an E-cad^{KO} organoid, visualized by labeled nuclei (H2b-mNeon)

Movie S5. Example of a perpendicular cell division (marked by a yellow arrowhead) in an E-cad^{KO} organoid, visualized by labeled nuclei (H2b-mNeon)

Movie S6. Three-dimensional visualization of a perpendicular cell division (marked by a yellow arrowhead) in an E-cad^{KO} organoid, visualized by labeled nuclei (H2b-mNeon)

Movie S7. Example of a daughter cell from misoriented division in an E-cad^{KO} organoid that is mispositioned basally and reintegrates in the epithelial layer (highlighted by a yellow box)

Movie S8. Example of a daughter cell from misoriented division in an E-cad^{KO} organoid that is mispositioned apically and reintegrates in the epithelial layer (highlighted by a yellow box)

Movie S9. Example of an E-cad^{KO} organoid that progressively loses its epithelial monolayer due to apically mispositioned daughter cells that fail to reintegrate (one example is highlighted by a yellow box)

Movie S10. Example of an E-cad^{KO} organoid with a disseminating cell due to a mispositioned daughter cell (highlighted by a yellow box) after the monolayer is lost

Movie S11. Example of an E-cad^{KO} organoid with a disseminating cell due to a mispositioned daughter cell that had already partially delaminated upon entry into mitosis (highlighted by a yellow box)

Movie S12. Example of an E-cad^{KO} organoid with a non-mitotic cell being extruded from the epithelium (highlighted by a yellow box)

Movie S13. Example of a disseminated E-cad^{KO} cell that progressively develops into an SRC-like cell